

THE AC FIELD EFFECT IN GERMANIUM WHISKERS

by

GERALD PAUL HART

B.S., Creighton University, 1963

---

A MASTER'S THESIS

submitted in partial fulfillment of the

requirements for the degree

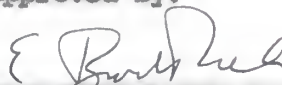
MASTER OF SCIENCE

Department of Physics

KANSAS STATE UNIVERSITY  
Manhattan, Kansas

1966

Approved by:



---

Major Professor

LD  
2668  
T4  
1966  
H326  
C.2  
Document

TABLE OF CONTENTS

INTRODUCTION . . . . .	1
WHISKER GROWTH . . . . .	2
THEORY . . . . .	5
EXPERIMENTAL TECHNIQUES . . . . .	17
EXPERIMENTAL RESULTS . . . . .	25
DISCUSSION . . . . .	35
ACKNOWLEDGMENT . . . . .	42
REFERENCES . . . . .	43

## INTRODUCTION

In the last five years, a number of investigators have observed semiconductor whisker growth; however, few attempts have been made to study their properties. Ruth, Marinace, and Dunlap (9), in a study of the growth of single-crystal germanium layers by the method of epitaxy, noted the growth of whiskers under certain conditions; however, a study of their properties was not attempted. One group of workers (10), has reported resistivity and mechanical deformation measurements. Room-temperature resistivities of approximately 40 ohm-cm and whisker radii of 15 to 50 microns were observed. Owing to their small diameter, the surface area-to-volume ratio of the whiskers is quite large ( $10^3$  to  $10^4/\text{cm}$ ), so that surface phenomena tend to be strongly in evidence. Furthermore, the fact that the whiskers are usually bounded by crystal planes suggests that measurements of their surface properties may be interpretable in more detail than has been achieved with polished and etched bulk specimens.

One of the methods for investigating surface phenomena in semiconductors is the field effect, which is the change in the conductance of a semiconductor that occurs when an electric field is capacitively applied to its surface. In this paper, the techniques involved in ac field effect measurements on germanium whiskers and the results obtained by this method are reported.

## WHISKER GROWTH

A germanium di-iodide ( $\text{GeI}_2$ ) disproportionation method was used to grow germanium whiskers (9). This process involved the formation of  $\text{GeI}_2$  followed by its decomposition to germanium tetra-iodide ( $\text{GeI}_4$ ) and free germanium atoms, according to the reaction:



The reaction chamber, constructed of pyrex glass tubing, was situated in an oven having two independently-controlled temperature regions. The formation of  $\text{GeI}_2$ , resulting from the reaction of germanium and iodine vapor, took place in the high temperature region ( $650^\circ$ ). For this reaction, chips of high resistivity germanium, etched in CP-4, were located in the reaction chamber, as indicated in Fig. 1. Iodine vapor, sublimated three times to insure purity, and an inert carrier gas (argon) were introduced into the high temperature region of the chamber through an opening on the left. As the gaseous  $\text{GeI}_2$  was carried into the lower temperature region ( $400^\circ\text{C}$ ), decomposition occurred. To provide nucleation sites for the free germanium atoms, a germanium substrate was inserted at the end of this region. The substrate was initially prepared by depositing films of germanium on a glass slide; the deposit was seeded with tellurium powder and the seeded substrate was then etched in CP-4. The required environment for whisker growth was found to be extremely dependent on the iodine vapor pressure, the substrate temperature, and

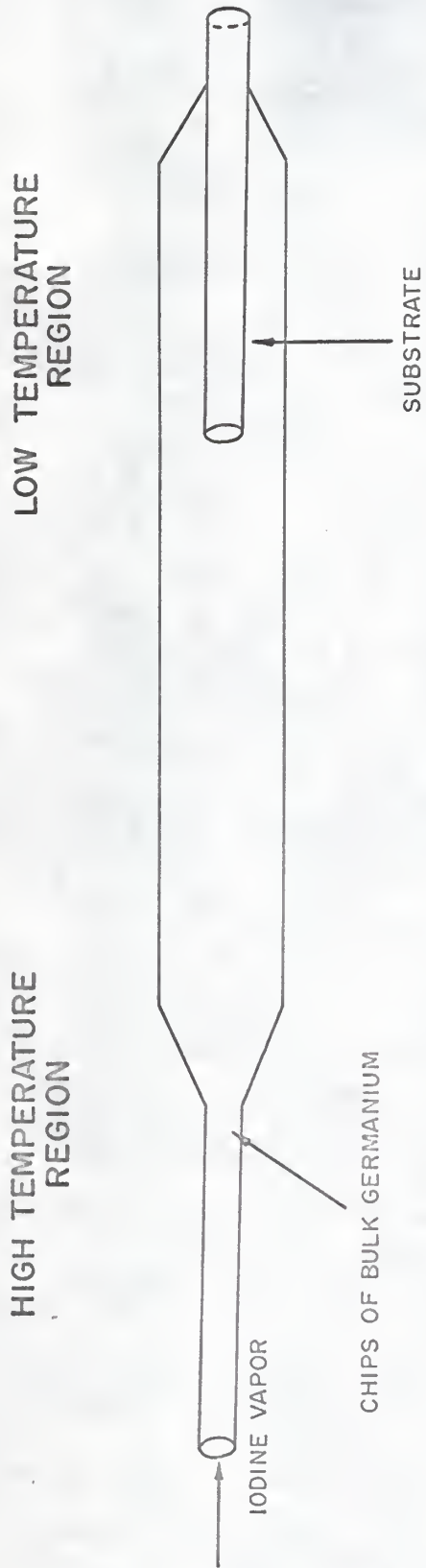


Fig. 1. The germanium di-iodide disproportionation reaction chamber used for growing germanium whiskers.



the substrate preparation. Many attempts were made to grow whiskers on a pure germanium substrate; however, the only large whisker growth occurred when a tellurium-doped substrate was used. Similar findings have been reported in attempts to grow silicon whiskers (13).

Whisker growth occurred on the first six centimeters of the substrate; the growth appeared to be the most dense on and near the end of the substrate tube. The majority of the whiskers were clustered about nucleation sites on the substrate; some, however, appeared to have grown from sites on other whiskers. Dimensional measurements were made on a number of the whiskers; the average length was found to be about three millimeters; measured radii varied from one to seven microns. The whiskers of the smaller radii appeared to be cylindrical, while those with a thickness greater than about four microns were observed to have a rectangular cross-section. Pits resembling etch pits were noticed on the surfaces of the larger whiskers; these may have been etched out by excess iodine vapor during the cooling period subsequent to whisker growth.

Rotation patterns were taken on two selected specimens, W-2 and W-3. An analysis confirmed the assumed germanium structure of the whiskers and indicated for both specimens a  $(2\bar{1}1)$  growth axis.

## THEORY

The electrical conductivity of a semiconductor is given by the equation:

$$\sigma = q(\mu_n n_0 + \mu_p p_0) \quad (1)$$

where  $q$  is the electronic charge,  $n_0$  the electron concentration,  $p_0$  the hole concentration,  $\mu_n$  and  $\mu_p$  are the bulk mobilities for electrons and holes, respectively. For a sufficiently strong n-type semiconductor, the term involving the hole concentration is negligible, and Eq. (1) can be written:

$$\sigma = q\mu_n n_0 \quad (2)$$

If the electron mobility is known, the electron concentration can then be determined as a function of the resistivity  $\rho$  of the sample:

$$\begin{aligned} n_0 &= \sigma / q\mu_n \quad (3) \\ &= 1/\rho q\mu_n \end{aligned}$$

If the semiconductor is not too strongly n-type or p-type, Boltzmann statistics apply and the electron concentration can be described in terms of the departure from intrinsic conditions by the equation:

$$n_0 = n_i e^{q\phi/kT} \quad (4)$$

where  $n_i$  is the intrinsic carrier concentration,  $k$  is Boltzmann's

constant,  $T$  is the absolute temperature, and  $\phi$  is the electrostatic potential, i.e. the potential difference between the intrinsic Fermi energy level,  $E_i$ , and the Fermi energy level,  $E_f$ .  $\phi$  is considered positive if  $E_i$  lies below  $E_f$ , as in the case of an n-type semiconductor. Using (3) and (4) the electrostatic potential may be expressed in terms of the resistivity:

$$\phi = \frac{kT}{q} \ln(n_0/n_i) \quad (5a)$$

The electrostatic potential in the interior of a semiconductor is denoted by  $\phi_b$ . Thus, from (5a) and (3):

$$\phi_b = -\frac{kT}{q} \ln(n_i q \mu_n \rho) \quad (5b)$$

The charge induced per unit area,  $Q_t$ , on the plate of a capacitor, of capacitance  $C$  per unit area, is given by the equation:

$$Q_t = CV \quad (6a)$$

where  $V$  is the potential difference between the capacitor plates. For a cylindrical capacitor, with a potential  $V$  between the electrodes, the instantaneous induced charge per unit area is:

$$Q_t = \frac{k\epsilon_0}{a \ln(b/a)} V \quad (6b)$$

where  $\epsilon_0$  is the electrical permittivity constant,  $k$  the dielectric constant,  $a$  the inner electrode radius, and  $b$  the outer electrode radius.

At the surface of a semiconductor, there exists additional allowed energy states. Various origins of these surface states



are recognized: termination of the lattice (Tamm states), imperfections in the crystalline surface, and atomic or molecular impurities. Generally, some of the allowed surface states, which may be of either the acceptor or donor type, will lie below the Fermi level at the surface. In the case of an n-type semiconductor with acceptor-type surface states, electrons in the conduction band at the surface will tend to drop into these states of lower energy. Due to the resulting depletion of electrons in the conduction band near the surface, a charge gradient, extending into the bulk, will be set up. Two opposing effects occur due to this redistribution of charge. First, as a result of the depletion of electrons in the conduction band (and the augmentation of the hole concentration in the valence band), there is a diffusion of electrons opposite to the electron concentration gradient, i.e. from the bulk toward the surface, and a diffusion current of holes away from the surface into the bulk. Second, as a result of the excess negative charge trapped in surface states, there is an electrostatic field which causes electrons to move away from the surface into the bulk and holes to move from the bulk toward the surface. At equilibrium these two effects - the electrostatic field (or potential gradient) and the concentration gradient - nullify each other. At every point in the semiconductor the drift current of electrons up the potential gradient is exactly equal and opposite to the diffusion current of electrons down the electron concentration gradient, and the drift and diffusion currents of holes are likewise equal and opposite. The unbalanced charge, and hence

the currents, approach zero a short distance beneath the surface. The region in which they are nonzero is known as the space-charge region.

The energy bands in the space-charge region are bent, as shown in Fig. 2. Their slope is equal to the electrostatic field discussed above. It can be seen, as implied in Fig. 2, that the energy difference between the Fermi level and either the conduction or the valence band at the surface is just  $q\phi_D$  plus or minus the energy difference between  $E_i$  and  $E_c$  or  $E_v$ .

When an electric field is capacitively applied to the surface of a semiconductor, a charge is induced on or near its surface. At equilibrium the induced charge appears partly as a change in the net space charge and partly as a change in the trapped surface state charge <sup>(3)</sup>. The total induced charge per unit area,  $Q_t$ , is then written as the sum of these terms:

$$Q_t = Q_{sc} + Q_{ss} \quad (7)$$

where  $Q_{sc}$  is the induced charge per unit area appearing in the space-charge region, and  $Q_{ss}$  is that part appearing in the surface states.

If the external field is applied suddenly, the induced charge appears first in the space-charge region, and then begins an approach to equilibrium; the rate at which equilibrium is restored depends on the magnitude of the mean life associated with the filling or emptying of the surface states.

Field effect measurements involve measuring the change in conductance corresponding to the altered space-charge concen-

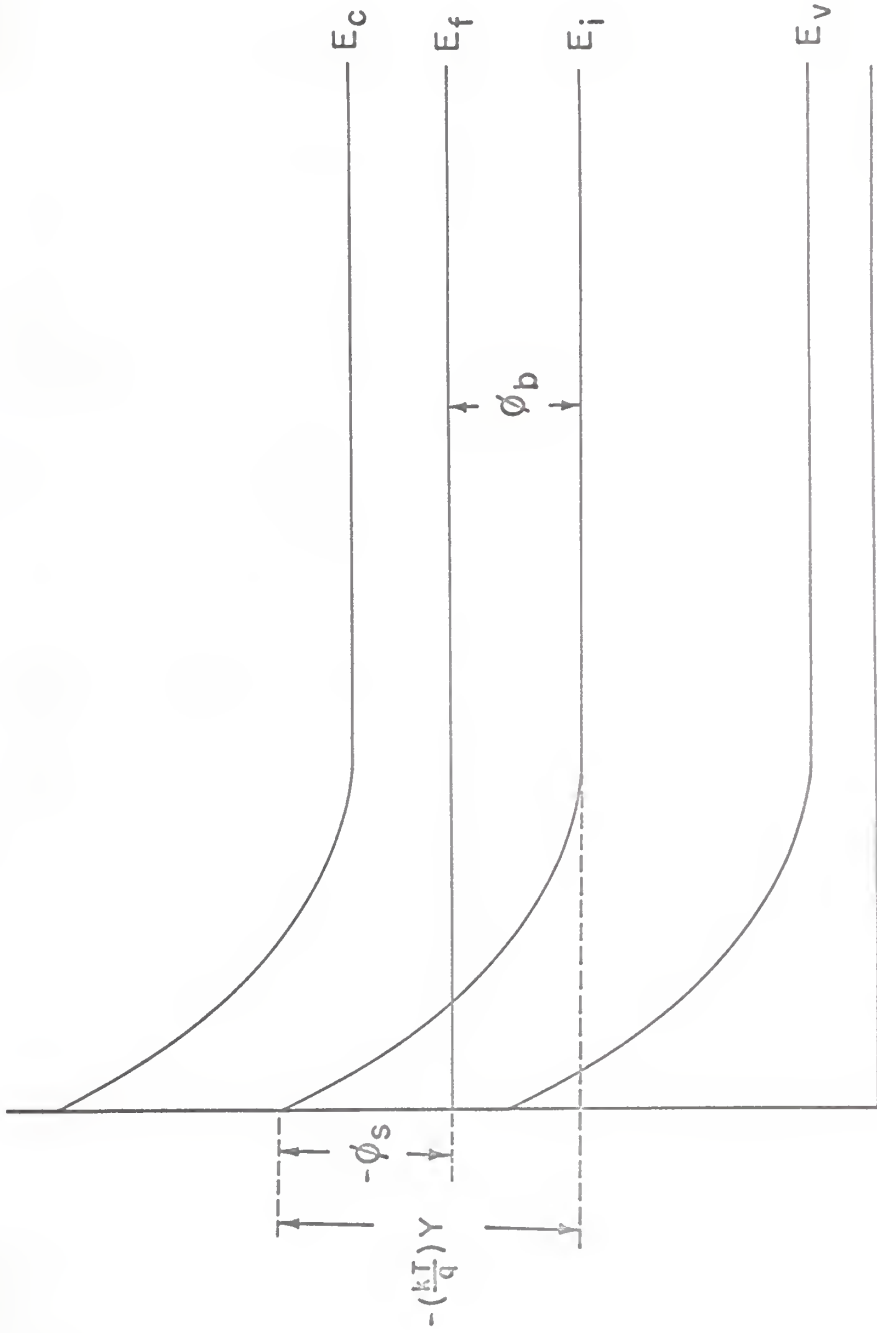


Fig. 2. The energy band diagram for a n-type semiconductor with a depletion-type space-charge region.



trations as a function of the total induced charge. However, only that portion of the induced charge remaining in the space-charge region,  $Q_{SC}$ , contributes to the change in the conductance; the induced charge appearing in the surface states is assumed immobile (3).

The conductance of the space-charge region, called surface conductance, is defined as the change in conductance per square of surface area relative to the flat band condition\* (no space charge) at the surface, and is given by:

$$\Delta G = q(\mu_n^i \Delta N + \mu_p^i \Delta P) \quad (8)$$

where  $\Delta N$  and  $\Delta P$  are the changes in the carrier concentrations in the space-charge region relative to the flat band condition;  $\mu_n^i$  and  $\mu_p^i$  are the effective mobilities of the electrons and holes, respectively.

If the experimental conductance change can be related to the corresponding change in the space-charge,  $Q_{SC}$ , one can then determine the induced surface state charge,  $Q_{SS}$ , using Eq. (7), provided the total induced charge is known. The general procedure followed in relating the surface conductance,  $\Delta G$ , to the space-charge,  $Q_{SC}$ , is similar to a method suggested by Bankury, Low, and Nixon (2). Briefly, one determines  $\Delta N$ ,  $\Delta P$ ,  $\mu_n^i$  and  $\mu_p^i$  as a function of  $\beta_s$ , the electrostatic potential at the surface ( $\beta_s$  represents the separation between the Fermi energy level and

\*Note that by virtue of this definition,  $\Delta G$  is, in general, non-zero when the external field is zero.



the intrinsic Fermi energy level at the surface, as shown in Fig. 2). Then, by use of Eq. (8), the surface conductance can be evaluated for various values of  $\beta_s$ . Likewise,  $\Omega_{sc}$  is determined as a function of  $\beta_s$ ; and thus, one can find  $\Delta G$  and the corresponding  $\Omega_{sc}$  for common values of  $\beta_s$ .

The expressions used in relating  $\Delta N$ ,  $\Delta P$ , and  $\Omega_{sc}$  to  $\beta_s$  are due to Kingston and Neustadter <sup>(6)</sup>. Nondegenerate statistics and completely ionized impurity levels are assumed. The derivation consists of solving Poisson's equation, with boundary conditions appropriate to the space-charge region, to obtain the internal electric field at the surface. Then, by using Gauss's law, the space charge necessary to produce this field is determined. The carrier concentrations are then found by integrating the charge carrier distributions over the space-charge region. The expressions obtained are:

$$\Omega_{sc} = 2qn_i L_D F(u_s, u_b) \quad (9)$$

$$\Delta P = n_i L_D G(u_s, u_b) \quad (10)$$

$$\Delta N = n_i L_D G(-u_s, -u_b) \quad (11)$$

with  $u_s = q\beta_s/kT$  and  $u_b = q\beta_b/kT$

where  $L_D$  is the Debye length. The functions  $F(u_s, u_b)$ ,  $G(u_s, u_b)$ , and  $G(-u_s, -u_b)$  have been evaluated by these authors, using  $u_s$  as a parameter for various values of the bulk potential.

The effective mobilities in Eq. (8) are generally less than the corresponding bulk values due to surface scattering. For

the case of diffuse surface scattering, this reduction in mobility becomes significant when the width of the space-charge region is comparable or less than the mean free path of the charge carriers (11). There has been some question as to whether the surface scattering is diffuse or specular. If the scattering were specular, there would be no reduction in the mobility, since only the normal component of the carriers' momentum would be reversed. However, for diffuse surface scattering, the charge carriers upon being scattered, effectively, would have their free paths and velocities terminated (1).

Expressions for the effective mobilities as a function of  $u_s$  have been calculated for germanium by Greene, Frankl, and Zemel (5). These authors have considered two cases: a thin slab with partly diffuse and partly specular surface scattering, and a thick slab (thickness much greater than  $L_D$ ) with diffuse surface scattering. Nondegenerate statistics, a constant relaxation time, and a constant effective mass are assumed. The derivation for the case of a thick slab begins by solving Boltzmann's equation for an electron distribution in the presence of a small electric field, with the appropriate boundary conditions. The effective mobility is defined in terms of an integrated current density across the sample. Further manipulation, along with the above expressions for  $\Delta N$  and  $\Delta P$ , yield the following equations:

$$\mu_n^i / \mu_n = 1 - \frac{(\exp u_b) (\lambda_n / L_D)}{G(-u_s, -u_b)} [\exp(u_s - u_b) - 1] \quad (13)$$

$(u_s \approx u_b)$

$$\mu_n'/\mu_n = 1 - \frac{(\exp u_b) (\lambda_n/L_D)}{G(-u_s, -u_b)} K(u_s, u_b) \quad (14)$$

$(u_s \geq u_b)$

The corresponding equations for the effective hole mobilities are obtained by replacing  $u_s$  by  $-u_s$ ,  $u_b$  by  $-u_b$ , and  $n$  by  $p$  in the above expressions. Values of these mobility ratios as a function of  $u_s$  have been numerically evaluated by these authors for various bulk potentials.

By the use of these calculations for the effective mobilities and those for  $\Delta N$  and  $\Delta P$ , the change in surface conductance, as given by Eq. (8), can be numerically evaluated as a function of  $u_s$  for a given value of the bulk potential. The space charge as a function of  $u_s$  is obtained from Eq. (9). A curve, obtained in this manner, relating  $\Delta G$  and  $\Omega_{SC}$  for germanium at 300°K with  $u_b = 7.0$  is shown in Fig. 3.

It is convenient at this point to introduce the parameter  $Y$ , called the surface potential, which is defined as a dimensionless potential associated with the bending of the energy bands in the space-charge region; it is related to the electrostatic potential  $u_s$  by the equation:

$$Y = (q/kT) (\beta_s - \beta_b) \quad (15)$$

The values of  $Y$ , obtained from the known values of  $u_s$  and  $u_b$ , are indicated along the theoretical curve in Fig. 3.

In measuring the ac field effect, one obtains directly an experimental curve showing conductance as a function of the applied potential. Knowing the capacitance of the whisker-field

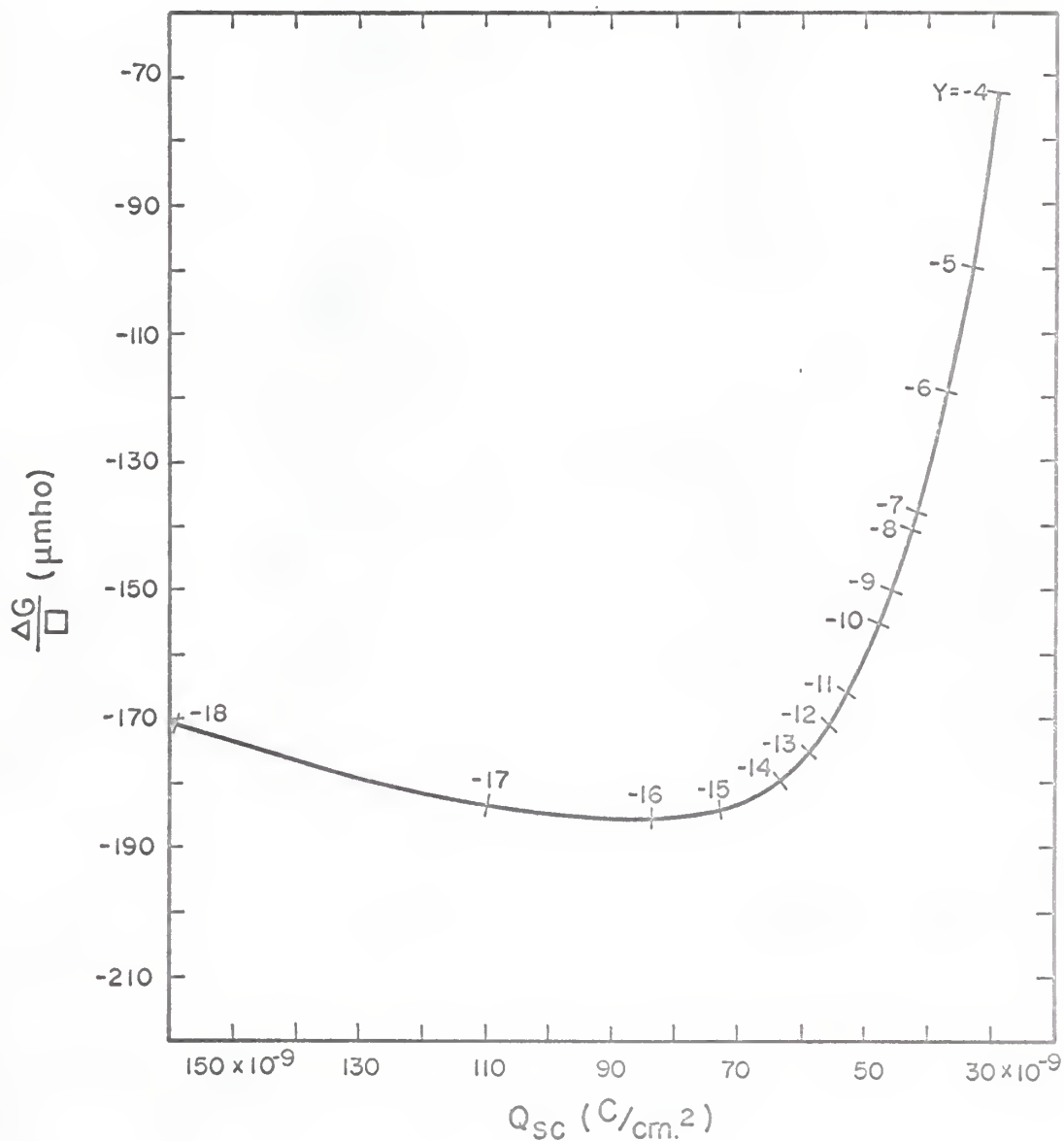


Fig. 3. The theoretical surface conductance as a function of the space charge for n-type germanium with a bulk potential of 0.19 eV at 300°K.



electrode combination, one then obtains the change in conductance as a function of the total induced charge,  $Q_t$ . The induced surface state charge can be determined along the experimental curve, by use of Eq. (7), provided the induced space-charge,  $Q_{sc}$ , which results in the experimental surface conductance, is known. The relationship between the experimental conductance and the corresponding induced space charge can be established if a minimum is observed in the experimental curve. At the conductance minimum, from Eq. (8), one obtains:

$$\delta(\Delta G) = \delta(q\mu'_n \Delta N + q\mu'_p \Delta P) = 0$$

In principle, by substitution of the expressions for the carrier concentrations and the effective mobilities into the above equation, one can obtain a value of the surface potential in terms of the bulk concentrations and bulk mobilities (4). Thus, at the conductance minimum, the surface potential is uniquely determined by the bulk properties. Such an evaluation, however, would prove extremely tedious due to the complicated nature of the mobility expressions. From Eq. (9) it can be shown that the space charge,  $Q_{sc}$ , in a given semiconductor, is a single-valued function of the surface potential. Thus, at the minimum of the conductance curve,  $Q_{sc}$  is likewise uniquely determined by bulk properties. As previously indicated, if the bulk properties are known, a theoretical relationship between  $\Delta G$  and  $Q_{sc}$  can be determined. At the minimum of this theoretical curve, the value of  $Q_{sc}$  is a unique function of the bulk properties. Thus, the

value of  $Q_{sc}$  at the experimental minimum is equal to the value of  $Q_{sc}$  at the theoretical minimum. Although  $Q_{sc}$  has the same value at both minimums, the values of the surface conductance at these points will, in general, differ since the experimental conductance change is arbitrarily measured relative to its minimum. To give the experimental conductance values an absolute significance, one uses the fact that  $Q_{sc}$  is the same at both minimums and thus that the values of  $\Delta G$  should, likewise, be the same at both minimums\*; therefore, one adjusts vertically the minimum of the experimental curve to correspond with the minimum of the theoretical curve. Following this adjustment, the values of the surface potential and the induced space charge are given for the experimental curve by the values determined along the theoretical curve. The induced surface charge  $Q_{ss}$ , for a given value of  $\Delta G$  or the surface potential, is then  $Q_t - Q_{sc}$ .

Using such an analysis, one can determine the induced surface state charge and possibly obtain some information concerning the surface-state energy distribution.

\*Only the induced charge in the space-charge region,  $Q_{sc}$ , contributes to  $\Delta G$ .

## EXPERIMENTAL TECHNIQUES

For field effect measurements, a cylindrical capacitor was constructed with a whisker mounted as the inner electrode, as shown in Fig. 4. The outer cylinder was cut and formed from rolled out tin-lead solder. The cylinder was supported on a 1" x 3" glass microslide by thin glass blocks on each side. Slow-drying Elmer's Epoxy glue was used as a binding agent. Before the epoxy was allowed to set, the cylinder axis was aligned with the plane of the glass blocks. Approximately 24 hours was then allowed for drying.

Using fine-point tungsten probes, a whisker was removed from the substrate and inserted into the mounted cylinder. The portions of the whisker that extended beyond the ends of the cylinder were allowed to rest on the glass blocks. Further manipulation of the whisker was required to align the portion of the whisker in the cylinder along the cylindrical axis. To secure the whisker in position, fine threads of epoxy glue were laid across a portion of the ends of the whisker.

Electrical contacts were made to the whisker using an air-drying silver print. This type of contact was found to be non-ohmic as indicated by the voltage-current curves shown in Fig. 5. A number of contacts were also made by copper-plating the ends of the whisker and then applying silver print to the copper plating. However, no observable improvement in the non-ohmic behavior was achieved by using the more difficult plating method. Indium soldered-contacts were attempted, but problems were



Fig. 4. The field effect capacitor. The whisker was mounted as the center electrode of a cylindrical capacitor.



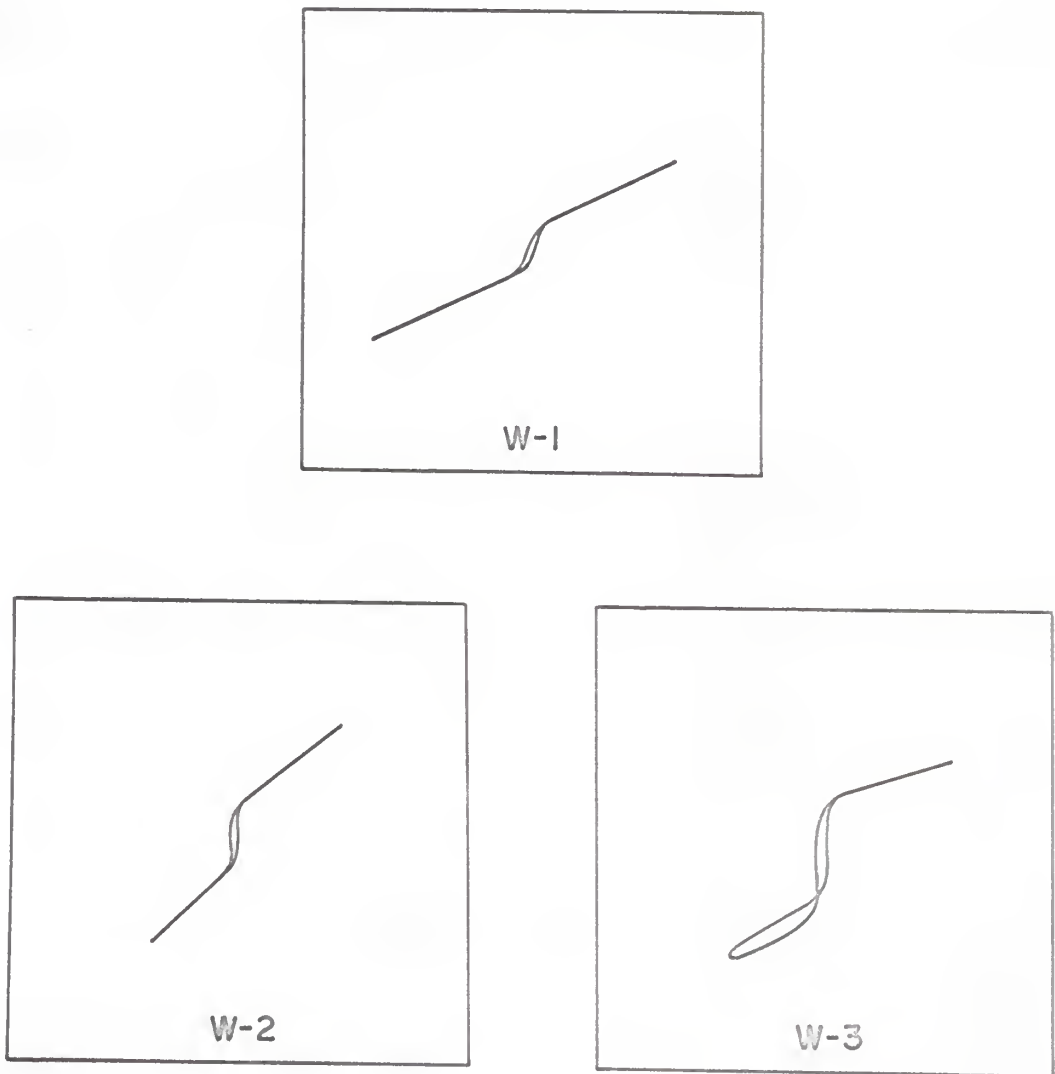


Fig. 5. The current-voltage characteristics of the whisker-to-metal contacts for the three specimens used for field effect measurements.

encountered with rapid oxidation and high surface tension of the molten indium. Other soldering agents proved equally unsuccessful.

To determine the bulk electrostatic potential, it was necessary to determine the whisker type and its resistivity. A thermal method was used in determining the sign of the majority carriers. Initially, contacts were made to a whisker mounted between the ends of two glass blocks. A fine nichrome wire, embedded in the base of one of the glass blocks, served as a heating element. A galvanometer was connected to the whisker leads to determine the polarity of the current flow. Since the majority carriers will diffuse away from the hot region, the semiconductor type can be known by determining the polarity of the hot region. A number of whisker types were checked by this method; all were found to be n-type. This result was expected due to the tellurium seeding of the substrate prior to whisker growth.

Two methods were used in determining the resistivity of the samples: the first method was a determination from current-voltage curves portrayed on an oscilloscope. Sketches of these curves for the three specimens used for field effect measurements, are shown in Fig. 5. To obtain current-voltage curves, a potential from an audio frequency generator was applied across the whisker and a 1000 ohm resistor in series, and to the vertical deflection input of an oscilloscope. The potential across the series resistor was applied to the horizontal input; the total resistance of the whisker was then calculated from the slope of branches of the current-voltage curves. In view of the

non-ohmic behavior of the electrical contacts, it was suspected that significant contact resistance may be present in the measured resistances. To obtain some estimate of this possible error in the resistivities, measurements were made on a number of samples by the former method and by a null-current probe method. For probe measurements, four electrical contacts were made to the whisker. A measured current was allowed to flow through the whisker via the outer two contacts. To determine the voltage drop across the inner contacts, a potentiometer was used. With additional measurements of the contact size and whisker length between the two inner probes, the resistivity was calculated. The resistivities measured in this manner are not subject to error due to contact resistance. The resistivities determined from the current-voltage curves were found to be about 16% greater than those obtained by the probe method.

The electrical circuit used for field effect measurements was a modified Low bridge <sup>(8)</sup>, as shown in Fig. 6. A 60 cps sinusoidal voltage of 100 to 500 volts was applied to the outer cylinder of the field effect capacitor and to the horizontal input of an oscilloscope. The bridge was used to balance out the voltage drop across the whisker due to the displacement current flowing through the field effect capacitor. To achieve this balance the resistors  $R_1$  and  $R_2$  were adjusted, without applying the dc sweeping current, until only a horizontal trace was seen on the oscilloscope screen. Conductance changes were observed by passing a dc current of a fraction of a milliampere through the balanced bridge. Any change in the whisker conduc-

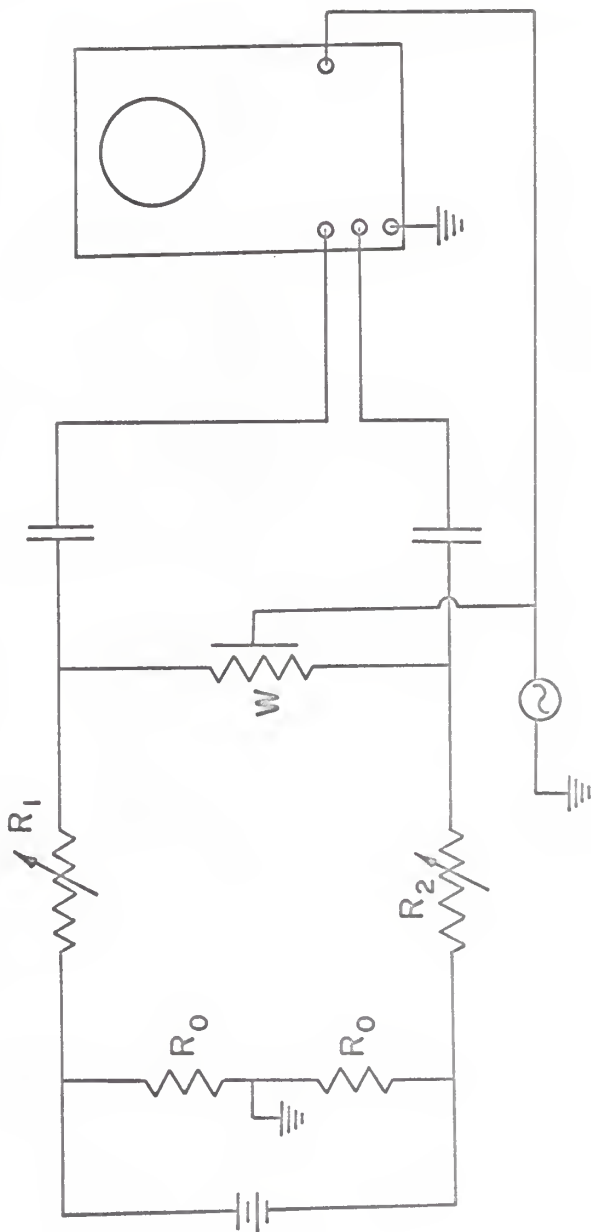


Fig. 6. Schematic diagram of the low bridge circuit for measuring the change in the voltage drop across the whisker as a function of the potential applied to the field effect capacitor.



tance resulted in a change in the voltage drop across the whisker and across the differential vertical input of the oscilloscope.

The change in whisker conductance is related to the voltage drop across the whisker by the equation:

$$\Delta G = \frac{R_1 + R_2 + R_w + R_1' + R_2'}{I R_w^2 (R_1 + R_2)} (-\Delta V) \quad (15)$$

where  $I$  is the dc sweeping current,  $R_w$  is the corrected whisker resistance,  $R_1'$  and  $R_2'$  are correction terms taking into account that portion of the whisker extending beyond the field effect capacitor, and  $\Delta V$  is the change in the voltage drop across the whisker associated with the external applied field. It should be noted that  $\Delta G$  is the total conductance change across the whisker, while the conductance change per square of surface area is:

$$\frac{\Delta G}{\square} = \Delta G \frac{L}{2\pi a} \quad (16)$$

where  $L$  is the effective whisker length and  $a$  the whisker radius. A correction was necessary to take into account that portion of the whisker extending beyond the ends of the field effect cylinder. The resistances of these portions,  $R_1'$  and  $R_2'$ , were calculated from measurements of the total whisker resistance, whisker length, and cylinder length assuming no capacitive fringe effects. The observed oscilloscope patterns represent the change in the voltage drop across the entire whisker (vertical axis) as a function of the sinusoidal potential applied to the field effect capacitor (horizontal axis). To relate the change in the

voltage drop across the entire whisker,  $\Delta V$ , to the corresponding change in conductance per square of surface area,  $\frac{\Delta G}{\square}$ . Eqs. (15) and (16) were used with the measured values of the constants. The total induced charge per  $\text{cm}^2$  was calculated using Eq. (6b). The capacitance of the field effect capacitor, which could not be measured due to the small size of the capacitor, was calculated from the geometry.

## EXPERIMENTAL RESULTS

Values of the bulk potential were calculated using Eq. (5b). The whisker type and resistivities were determined by the methods explained above. Room temperature values for the intrinsic concentration and the bulk electron mobility were obtained from Smith (12). The calculated resistivities and measured dimensions are given in Table I. Similar resistivity values for tellurium-doped germanium have been reported by Kosenko (7).

Table I. Dimensional measurements and bulk properties

W	whisker radius (microns)	cylinder radius (cm)	cylinder length (cm)	$\rho$ (ohm-cm)	$n_0$ (per cm <sup>3</sup> )	$u_b$
1	3.6	0.0991	0.277	0.065	$2.5 \times 10^{16}$	7.0
2	1.5	0.0678	0.145	0.032	$5.0 \times 10^{16}$	7.5
3	2.2	0.0668	0.150	0.039	$4.2 \times 10^{16}$	7.5

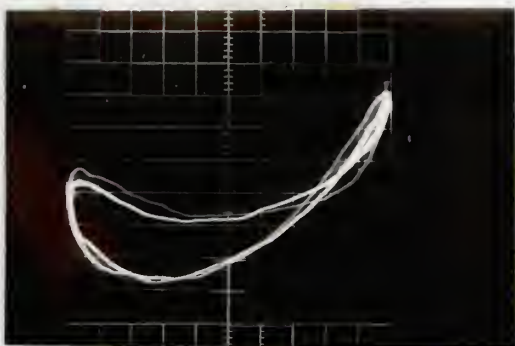
Photographs of the observed change in voltage drop across the whisker as a function of the potential applied to the field effect capacitor for three specimens are shown in Fig. 7. By appropriate changes of scale as indicated by Eqs. (15), (16), and (6b), these curves were interpreted as changes in the surface conductance as a function of the induced charge per unit area. The hysteresis noted in experimental conductance curves is believed to be associated with the non-ohmic nature of the metal-to-whisker contacts. Since it was not known with certainty which of the two curves represented the actual conductance change, the



W-1



W-2



W-3

Fig. 7. Oscilloscope patterns for the three specimens, showing the change in the voltage drop across the whisker as a function of the applied voltage.



surface state charge was determined for both curves.

To plot the experimental conductance curve along with the corresponding theoretical curve, the necessary adjustment in the vertical scale of the experimental curve was performed; this change in the experimental conductance scale, in order to align the minimums of both curves, was  $-184 \times 10^{-6}$  mho/ $\square$ . The plotted curves for three specimens are shown in Figures 8 through 13. With the experimental minimum having been adjusted, the values of the surface potential and of the induced charge in the space-charge region along the experimental curve correspond to the values indicated for the theoretical curve. The charge in the surface states for a given values of  $\Delta G$  or the corresponding surface potential was then found using the expression:

$Q_{SS} = Q_t - Q_{sc}$ . The change in the density of filled surface states  $N_{SS}$ , corresponding to a given value of the induced surface state charge  $Q_{SS}$ , is then just  $Q_{SS}/q$ . The induced surface state charge densities and the corresponding filled surface state densities are given in Table II, as a function of the surface potential.

Table II. Induced surface charge densities ( $C/cm^2$ ) and the corresponding filled surface state densities (per  $cm^2$ ) as a function of the surface potential.

Y	W-1		W-1	
	(lower curve)		(upper curve)	
	$Q_{ss} (x10^{-9})$	$N_{ss} (x10^{11})$	$Q_{ss} (x10^{-9})$	$N_{ss} (x10^{11})$
-13	-86	5.4	-	-
-14	-81	5.1	-76	4.8
-15	-75	4.7	-78	4.9
-16	-76	4.8	-60	3.8
-17	-87	5.4	-89	5.6

Y	W-2		W-2	
	(lower curve)		(upper curve)	
	$Q_{ss} (x10^{-9})$	$N_{ss} (x10^{11})$	$Q_{ss} (x10^{-9})$	$N_{ss} (x10^{11})$
-13	-	-	-	-
-14	-100	6.3	-106	6.6
-15	-68	4.3	-65	4.1
-16	-49	3.1	-47	2.9
-17	-59	3.7	-53	3.3

Y	W-3		W-3	
	(lower curve)		(upper curve)	
	$Q_{ss} (x10^{-9})$	$N_{ss} (x10^{11})$	$Q_{ss} (x10^{-9})$	$N_{ss} (x10^{11})$
-13	-82	5.1	-	-
-14	-76	4.8	-72	4.4
-15	-73	4.5	-82	5.1
-16	-74	4.6	-80	5.0
-17	-92	5.8	-92	5.8
-18	-137	8.6	-	-

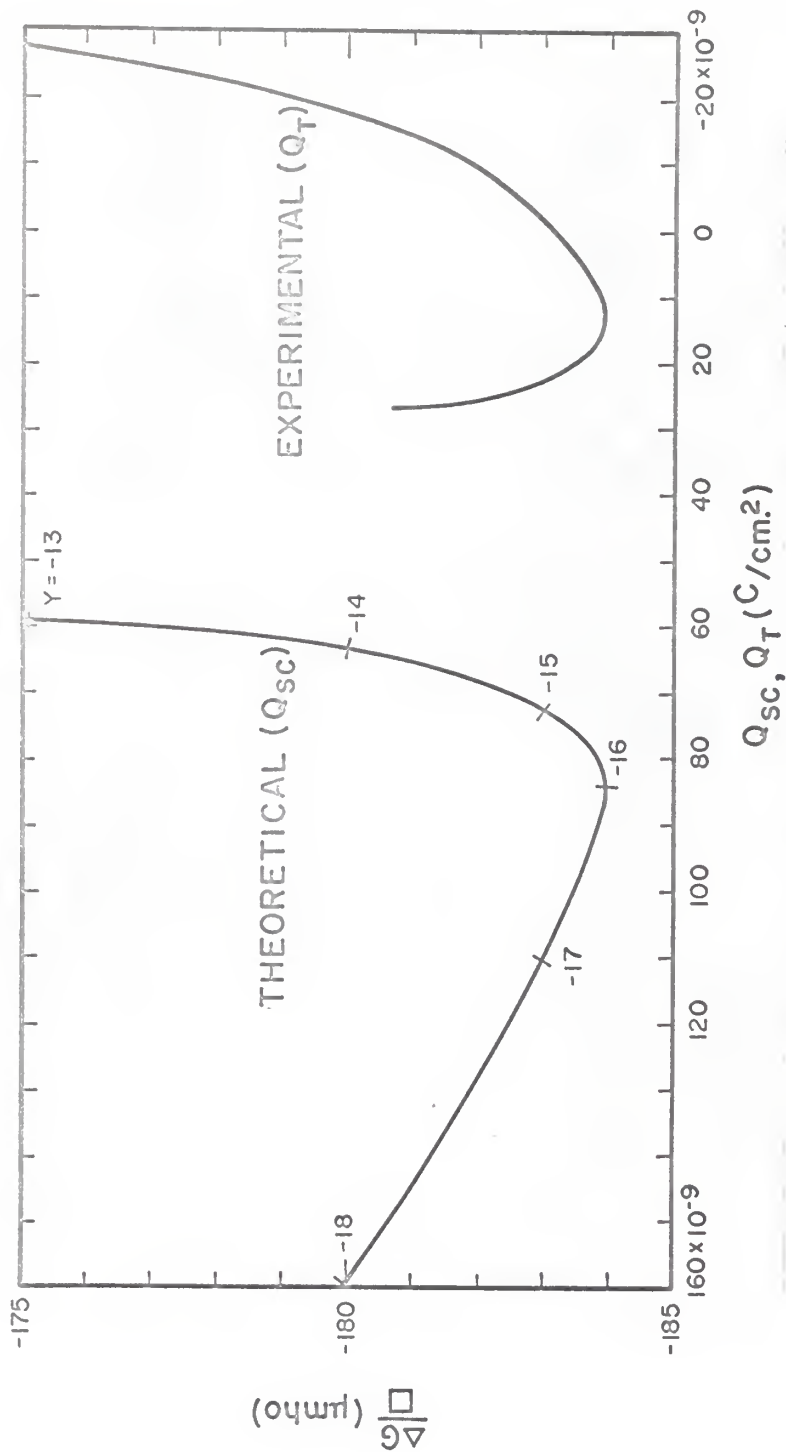


Fig. 8. The lower experimental conductance curve of W-1 with its minimum adjusted to the height of the theoretical conductance minimum.

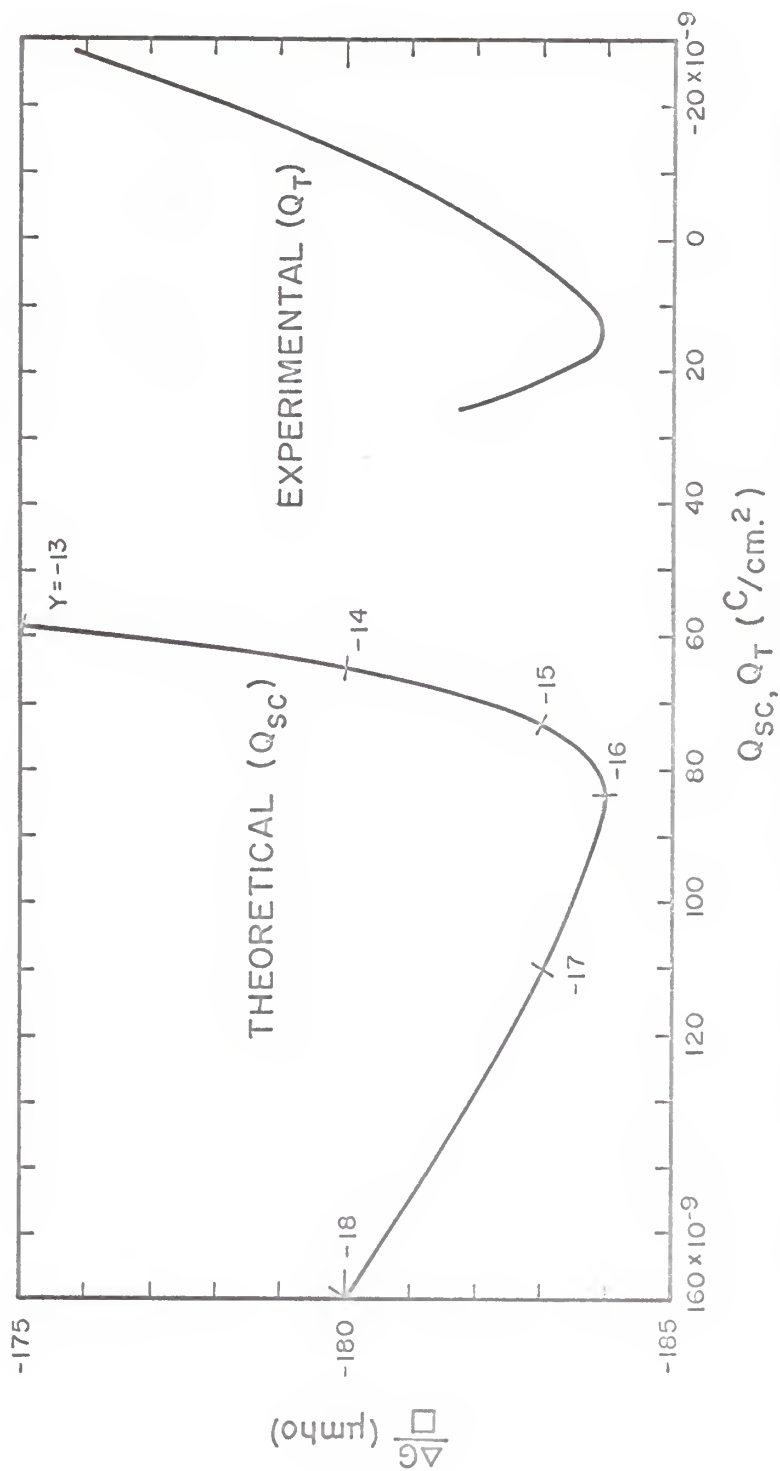


Fig. 9. The upper experimental conductance curve of W-1 with its minimum adjusted to the height of the theoretical conductance minimum.



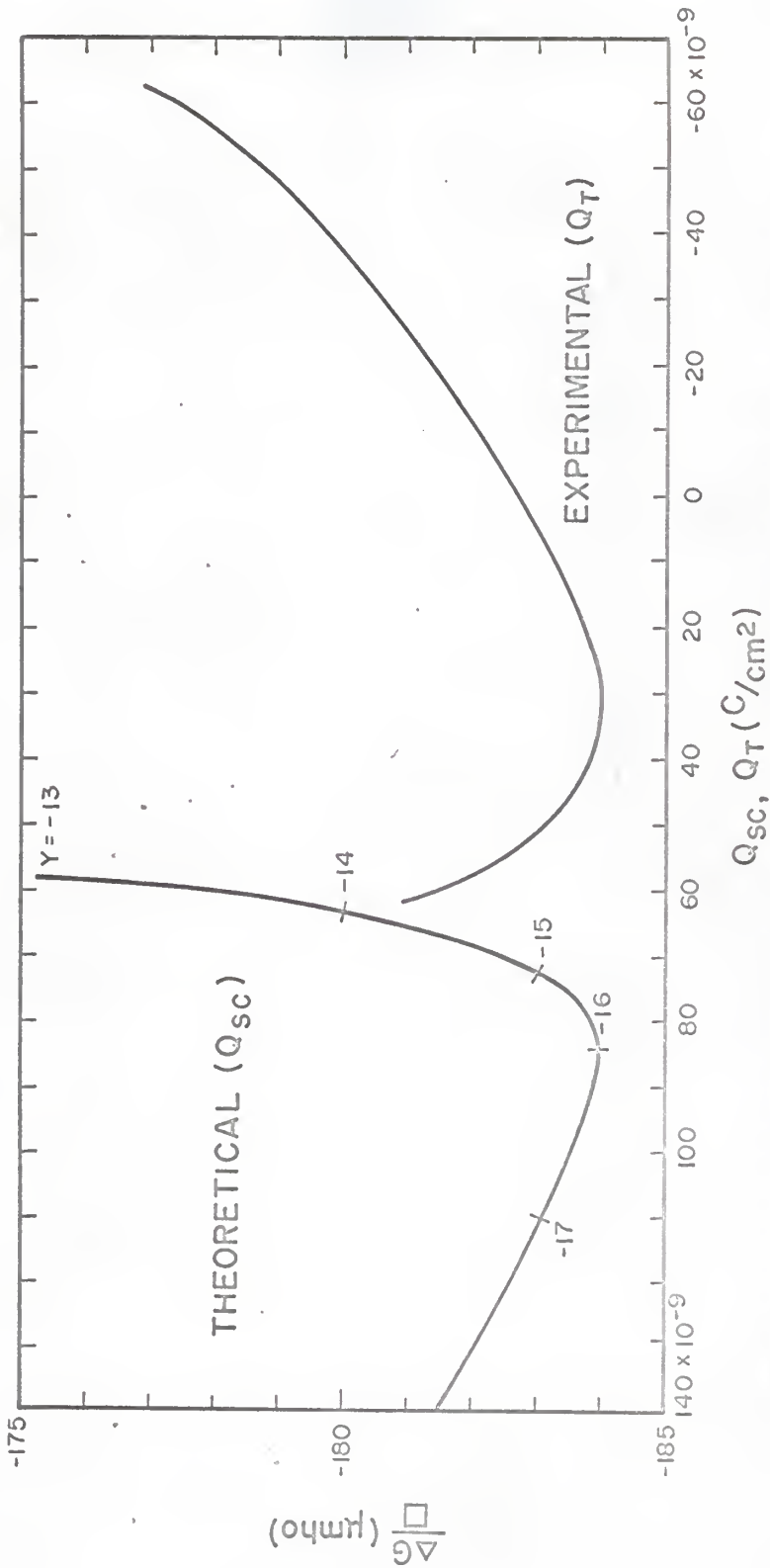


Fig. 10. The lower experimental conductance curve of W-2 with its minimum adjusted to the height of the theoretical conductance minimum.

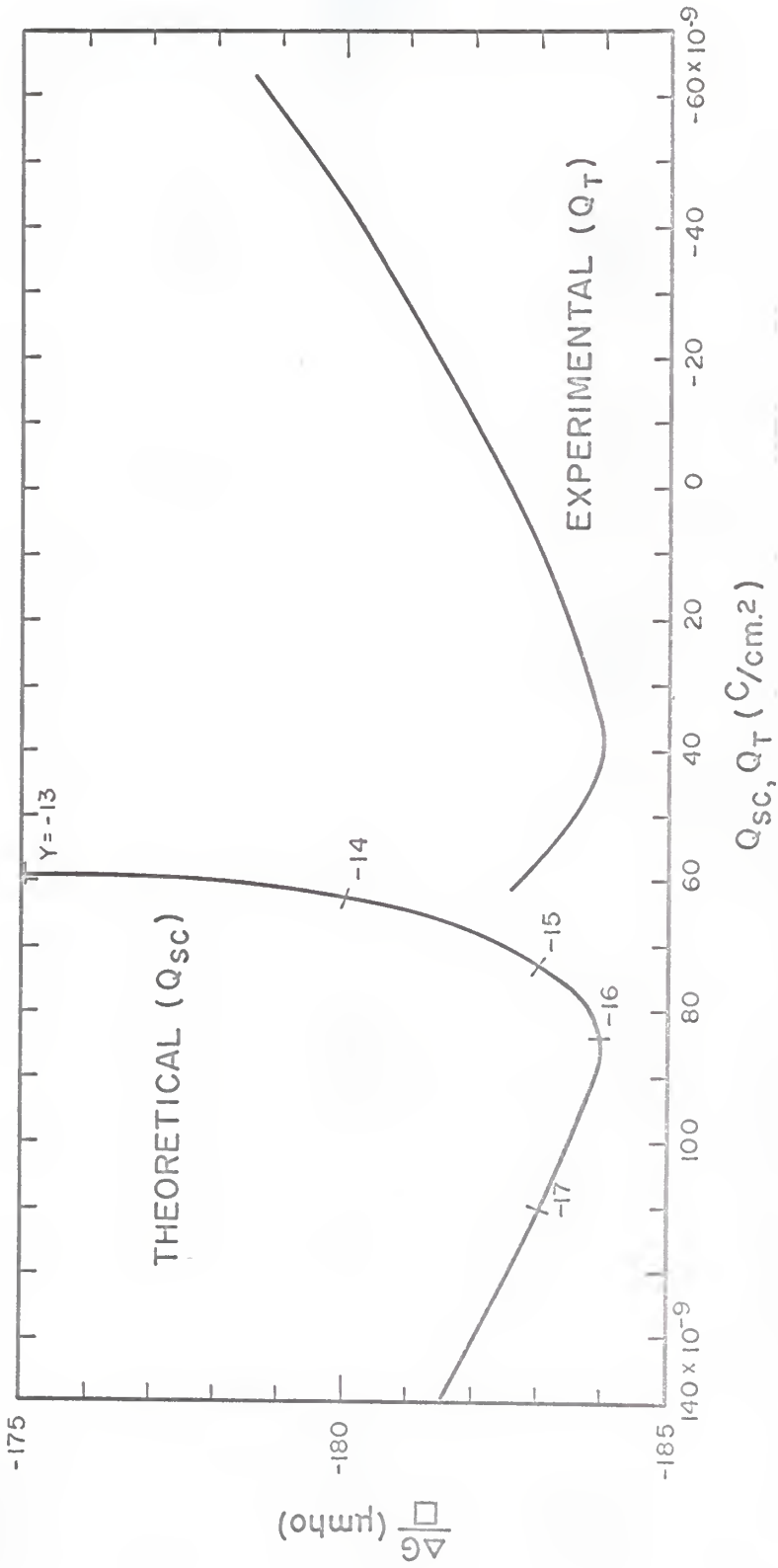


Fig. 11. The upper experimental conductance curve of W-2 with its minimum adjusted to the height of the theoretical conductance minimum.

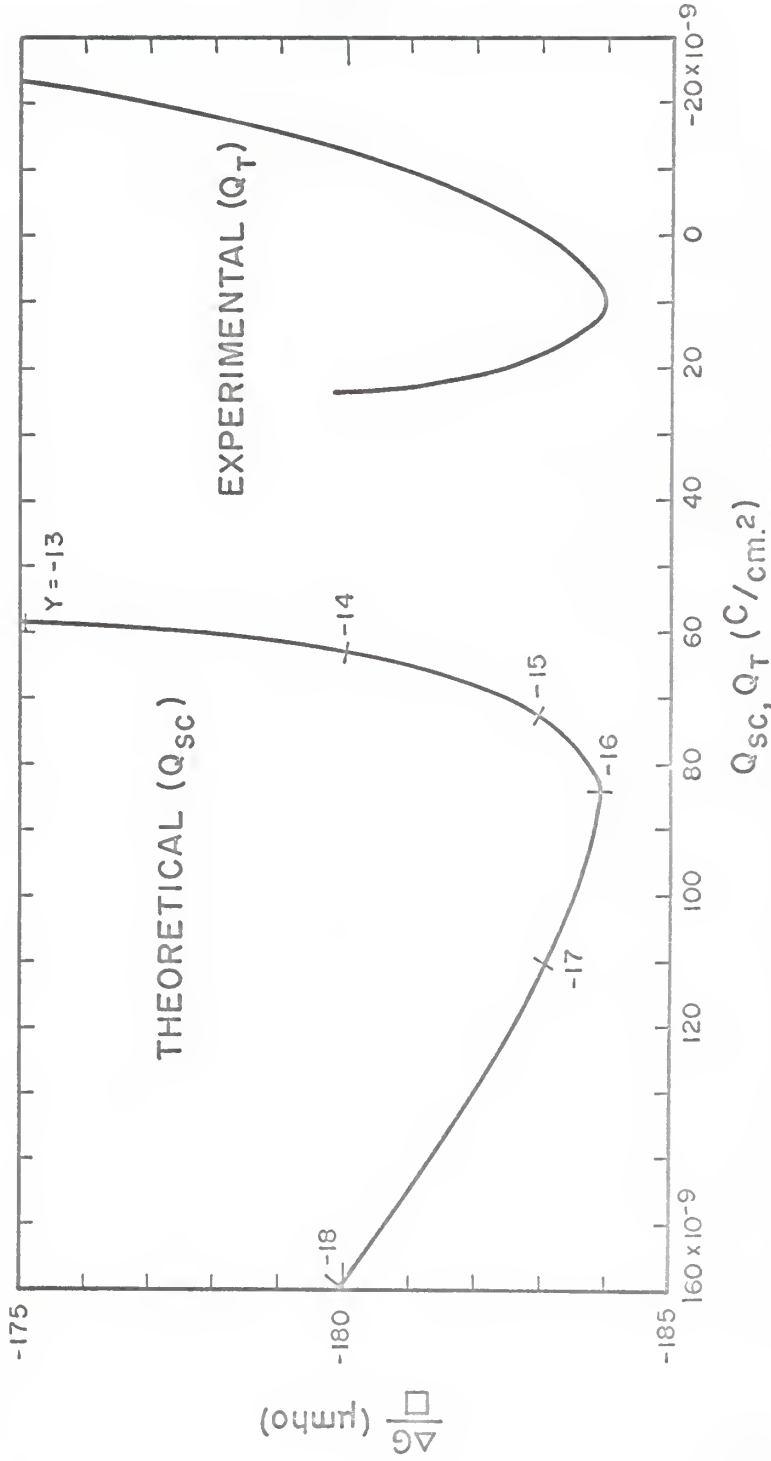


Fig. 12. The lower experimental conductance curve of W-3 with its minimum adjusted to the height of the theoretical conductance minimum.

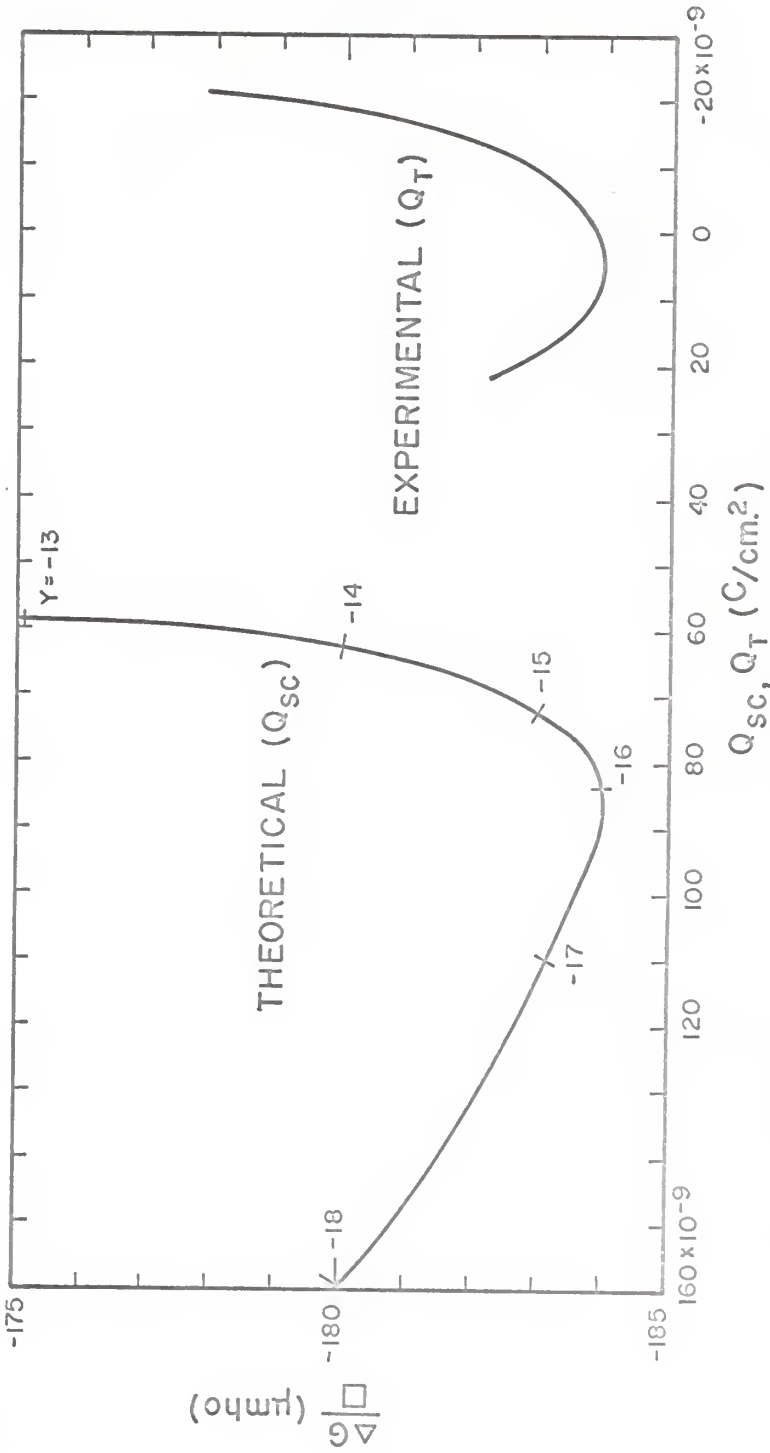


Fig. 13. The upper experimental conductance curve of W-3 with its minimum adjusted to the height of the theoretical conductance minimum.



## DISCUSSION

Before beginning an interpretation of the experimental results, the possible errors involved will be considered. In calculating the capacitance of the field effect capacitor, it was assumed that the whisker possessed a cylindrical cross-section. By using a high-power microscope, this assumption was observed to be valid at least to a first approximation for whiskers of a small radius (less than 4 microns). The assumed uniformity of the external electric field at the semiconductor surface is sensitive to deviation from the assumed cylindrical cross-section of the whisker. The electric field at abrupt surface discontinuities is quite large; however, such irregularities are usually the least accessible to current flow and, thus, do not significantly affect conductance changes. If, however, there are surface irregularities, which extend appreciably along the length of the whisker, a possible error in the observed conductance changes will arise from altered conduction along the irregularities; since the electric field is greater at points of surface discontinuities, the number of charges carries induced in such irregularities will likewise be greater, resulting in either a path of increased or decreased conductivity—depending on the space-charge type and the sign of the induced carriers.

The uniformity of the electric field at the surface of the whisker is also critically dependent on the symmetry of the mounted whisker in respect to the outer cylinder. Since this alignment was made visually, some error due to the lack of

perfect symmetry is undoubtedly involved. If the whisker is displaced slightly from the axis of the cylinder by only a translation perpendicular to its length, the resulting nonuniformity does not appreciably alter the observed conductance changes. However, if a misalignment is due to a slight rotation and translation of the whisker so that it is centered at one end but not the other, a differential charge density would be induced along the whisker. The voltage drop across the whisker due to the resulting current flow would be balanced out along with the voltage drop due to the displacement current. Any appreciable conductance change resulting from nonuniformly induced charge can be detected by noting changes in the shape of the conductance curve upon reversing the polarity of the dc sweeping voltage. The shape of the conductance curves of the mounted whiskers, used for measurements, did not display an observable dependence on the polarity of the dc sweeping voltage.

The measured radii of the whiskers are believed to be accurate to at least two places. Some question does arise, however, in the measurement of whisker length, since the location of the actual point of electrical contact in the silver is not known. It was assumed that the electrical contact was made at the tip of the contact. To obtain an estimation of the error involved, a number of successive length and resistance measurements were made on a given whisker by increasing the contact size after each measurement; a plot of the resistance as a function of the whisker length was found to be only approximately linear. If a constant contact resistance is assumed for each successive contact, one



can then conclude from such a plot, that some error is definitely involved in the length measurements.

An incorrect length measurement would result in an error in the calculated resistivities and, therefore, in the value of the bulk potential and in the calculation of  $\Delta G$  in Eq. (15). The bulk potential, since it is a logarithmic function of the resistivity, is not sensitive to slight errors in the resistivity. In calculating the surface conductance, such an error would be more significant, since it would involve not only the calculated sweeping current  $I$ , but also the correction terms  $R_1^i$  and  $R_2^i$ . However, these errors do not appear in the calculated surface state charges densities, since the experimental conductance curve is relative, that is, the experimental minimum is adjusted vertically to correspond with the theoretical conductance minimum.

The observed experimental conductance curves are shown in Fig. 7 for three specimens. The hysteresis, apparent in these curves, is believed to be primarily a result of the non-ohmic nature of the metal-to-whisker contacts. A comparison of the current-voltage curves and the experimental conductance curves indicates a correlation between the barrier height at the contacts and the degree of looping in the conductance curves; the looping appears to become more pronounced with increasing barrier heights. The direction of the horizontal sweep on the conductance curves was from the right (negative  $Q_t$ ) to the left (positive  $Q_t$ ) along the upper curve and from left to right on the lower curve. At the left end of these curves, where the conduction is due

primarily to minority carriers, one notes that the change in conductance, as the sweep reverses, is not as abrupt as on the majority carrier side; this is especially evident on the conductance curves for W-3. Since the minority carriers are supplied to the space-charge region by a generation process (holes cannot be supplied by the n-type bulk), a delay in this generation process could account for the looping. However, the exact nature of this phenomena is not known.

For the three specimens, these curves as shown in Figures 8 through 13, indicate a decrease in conductance for a decrease in the amount of induced negative charge. In this region, the space-charge layer is n-type, i.e. an exhaustion layer. At the left end of the conductance curves, an increase in the induced positive charge corresponds to an increase in conductance; thus, in this region, the space-charge layer is p-type, i.e. an inversion layer. At the minimum, the change in the surface conductance is zero: The conductance due to the changing hole concentration is balanced by the contribution due to the changing electron concentration. At this point, the space-charge region is effectively intrinsic. In the absence of an applied field,  $\Omega_t = 0$ , the space-charge region is n-type; this is indicated by the position of the point, corresponding to  $\Omega_t = 0$ , on the experimental conductance curves.

The relatively large separation between the theoretical conductance minimum and the experimental conductance minimum is attributed to the high density of surface states. If there were no surface states, the experimental and theoretical curves would



exactly superimpose; their presence, however, shifts the minimum of the experimental curve along the induced charge scale.

The induced surface charge densities are given in Table II, along with the corresponding densities of filled surface states. Because of the hysteresis in the conductance curves, these densities were determined for each branch of the hysteresis. However, only a small difference is detected, when the densities resulting from corresponding upper and lower curves are compared (except for W-1,  $Y = -16.0$ ). Thus, any error in the determined densities associated with this looping appears small.

The limited range of change in the surface potential does not allow significant conclusions to be made concerning the energy distribution of the surface states. The large changes in the induced surface state charge within the observed range does, however, suggest discrete levels of states.

The surface charge densities, at  $Q_t = 0$ , represent the case of no applied field. The value of the surface state densities, for this quiescent condition, were found to be approximately identical for the three specimens. This value,  $4.5 \times 10^{11}$  per  $\text{cm}^2$ , lies well with the range of reported surface state densities for germanium (3).

Under certain conditions many of the mounted whiskers showed anomalous field effect conductance curves. In most cases, an increase in the applied field or in the sweeping current, above certain values, resulted in a radical distortion of these curves. In particular, loops and sharp discontinuities appeared. To

examine the possibility that the discontinuities were due to field emission or current leakage from the surface, silicone oil was inserted in a few of the field effect capacitors. This dielectric was found to eliminate much of the anomalous behavior and to enhance the magnitude of the field effect; however, the looping on the minority carrier side of the conductance curve was also more prominent.

A number of the mounted whiskers failed to show any field-effect conductance change in the presence of a capacitively applied field. In these cases, a high noise level was usually observed with the sweeping current. It is believed that poor contacts were responsible for the noise level and the apparent absence of the effect.

Since the whiskers are of relatively small radii, one would expect a field effect of greater magnitude than was observed here; however, the width of the space-charge region and, thus the field effect, are greatly diminished by large impurity concentrations.

From these ac field effect measurements, filled surface state densities of  $10^{11}$  to  $10^{12}$  per  $\text{cm}^2$  were obtained for germanium whiskers. The relatively small changes in surface potential did not permit any detailed conclusions to be made concerning the energy distribution of these states. Further investigations of this effect in whiskers could possibly yield significant conclusions about the properties of surface states. However, the problems involved with the non-ohmic metal-to-whisker contacts and the difficulty in growing relatively pure

germanium whiskers must first be overcome.

## ACKNOWLEDGMENT

The author expresses his sincere gratitude to his major professor, Dr. E. Brock Dale, whose guidance and encouragement made this work possible. Indebtedness is acknowledged to Dr. R. Dean Dragsdorf for his assistance and constructive criticism of the manuscript.



## REFERENCES

1. Amith, A., Galvanomagnetic Properties of Semiconductor Thin Films and Surface Layers, *J. Phys. Chem. Solids*, 14, 271 (1960).
2. Banbury, P. C., Low, G. G. E., and Nixon, J. D., Semiconductor Surface Physics, edited by R. H. Kingston, (University of Pennsylvania Press, Philadelphia, 1957), p. 70.
3. Brown, W. L., Brattain, W. H., Garrett, C. G. B., and Montgomery, H. C., Semiconductor Surface Physics, edited by R. H. Kingston, (University of Pennsylvania Press, Philadelphia, 1957), p. 111.
4. Goldberg, Colman, Space Charge Regions in Semiconductors, *Solid State Electronics*, 7, 593 (1964).
5. Greene, R. F., Frankl, D. R., and Zemel, Jay, Surface Transport in Semiconductors, *Phys. Rev.*, 118, 967 (1960).
6. Kingston, R. H., and Neustadter, Siegfried F., Calculation of the Space Charge, Electric Field, and Free Carrier Concentration at the Surface of a Semiconductor, *J. Appl. Phys.*, 26, 718 (1955).
7. Kosenko, V. E., Two Simultaneously Acting Diffusion Mechanisms in Germanium, *Soviet Phy.--Solid State*, 3, 1526 (1962).
8. Low, G. G. E., Modulation of the Surface Conductance of Germanium and Silicon by External Electric Fields, *Proc. Phy. Soc. Lond.*, B, 68, 10 (1955).
9. Ruth, Ralph P., Marinace, John C., and Dunlap, Jr., W. C., Vapor-Deposited Single-Crystal Germanium, *J. Appl. Phys.*, 31, 995 (1960).
10. Sandulova, A. V., Bogoyavlenskii, P. S., and Dronyuk, M. I., Preparation and Some Properties of Whisker and Needle-Shaped Single Crystals of Germanium, Silicon, and Their Solid Solutions, *Soviet Phys. - Solid State*, 5, 1883 (1964).
11. Schrieffer, J. R., Effective Carrier Mobility in Surface Space Charge Layers, *Phys. Rev.*, 97, 641 (1955).
12. Smith, R. A., Semiconductors, (Cambridge University Press, London, 1959).

13. Wagner, R. S., Ellis, W. C., Jackson, K. A., and Arnold, S. M., Study of the Filamentary Growth of Silicon Crystals from the Vapor, *J. Appl. Phys.*, 35, 2993 (1964).

THE AC FIELD EFFECT IN GERMANIUM WHISKERS

by

GERALD PAUL HART

B.S., Creighton University, 1963

---

AN ABSTRACT OF A MASTER'S THESIS

submitted in partial fulfillment of the

requirements for the degree

MASTER OF SCIENCE

Department of Physics

KANSAS STATE UNIVERSITY  
Manhattan, Kansas

1966

Germanium whiskers were grown using a  $\text{GeI}_2$  disproportionation method. A X-ray analysis was made to determine structure and the growth axes of selected specimens. The whiskers were mounted as the center electrode of a cylindrical capacitor. Electrical contacts were made to the ends of the whiskers by means of a silver print. The current-voltage characteristics of the specimens revealed a non-ohmic behavior. To determine resistivities, dimensional measurements were made, and the total resistances were calculated from the slopes of the current-voltage curves. Due to the nature of the contacts, a large contact resistance was suspected. To obtain some estimate of this error, resistivities of other samples were determined from their current-voltage curves and by a null-current probe method. Since contact resistance is not involved in the latter method, a comparison should allow some estimate of the error. The resistivities, determined from the current-voltage curves, were found to be approximately 16% greater than those values obtained by the probe method.

From field effect measurements, the surface conductance was obtained as a function of the total induced charge,  $Q_t$ , for three whiskers. A theoretical determination of the surface conductance as a function of the induced charge appearing in the space-charge region,  $Q_{sc}$ , was made using the value of the bulk potential calculated from the measured resistivities of the specimens. Following a vertical adjustment of the experimental conductance minimum to the level of the theoretical



conductance minimum, the values of the surface potential and the space charge along the experimental curve were obtained from their values on the theoretical curve. Then for a given value of the surface potential, the induced surface state density was determined using  $Q_{ss} = Q_t - Q_{sc}$ . The densities of the filled fast surface states, corresponding to  $Q_{ss}$ , were found to range from  $10^{11}$  to  $10^{12}$  per  $\text{cm}^2$ . Some anomalous behavior was observed. A hysteresis in the conductance curve was noted. The origin of this phenomenon is not known, although some correlation between the contact barrier height and the amount of hysteresis is evident.